A Split Hopkinson Pressure Bar Technique to Determine Compressive Stress-strain Data for Rock Materials

by D. J. Frew, M. J. Forrestal and W. Chen

ABSTRACT—This paper presents a split Hopkinson pressure bar technique to obtain compressive stress-strain data for rock materials. This technique modifies the conventional split Hopkinson bar apparatus by placing a thin copper disk on the impact surface of the incident bar. When the striker bar impacts the copper disk, a nondispersive ramp pulse propagates in the incident bar and produces a nearly constant strain rate in a rock sample. Data from experiments with limestone show that the samples are in dynamic stress equilibrium and have constant strain rates over most of the test durations. In addition, the ramp pulse durations can be controlled such that samples are unloaded just prior to failure. Thus, intact samples that experience strains beyond the elastic region and postpeak stresses can be retrieved for microstructural evaluations. The paper also presents analytical models that predict the time durations for sample equilibrium and constant strain rate. Model predictions are in good agreement with measurements.

KEY WORDS—Hopkinson bar, pulse shaping, rock materials, high strain rate

The split Hopkinson pressure bar (SHPB) technique originally developed by Kolsky[1,2] has been used by many investigators to obtain dynamic compression properties of solid materials. The evolution of this experimental method and recent advances were discussed by Nicholas,[3] Follansbee,[4] Nemat-Nasser *et al.*,[5] Ramesh and Narasimhan,[6] Gray[7] and Gray and Blumenthal.[8] This technique has mostly been used to study the plastic flow stress of metals that undergo large strains at strain rates between $10^2 - 10^4\ s^{-1}$. As discussed by Yadav *et al.*,[9] data for the compressive flow stress of metals are typically obtained for strains larger than a few percentage points because the technique is not capable of measuring the elastic and early yield behavior. By contrast, most of the material behavior of interest for relatively brittle materials such as ceramics and rocks occurs at strains less than about 1.0 percent.

D. J. Frew is a Research Engineer, Structures Laboratory, Waterways Experiment Station, U.S. Army Engineer Research and Development Center, Vicksburg, MS 39180-6199. M. J. Forrestal (SEM Member) is a Distinguished Member of the Technical Staff, Sandia National Laboratories, Albuquerque, NM 87185-0303. W. Chen (SEM Member) is an Assistant Professor, Department of Aerospace and Mechanical Engineering, University of Arizona, Tucson, AZ 85721-0119.

Original manuscript submitted: February 10, 2000.
Final manuscript received: October 11, 2000.

In this study, we modified the conventional SHPB or Kolsky bar technique to obtain dynamic compressive stress-strain data for rock materials and conducted experiments with limestone samples that have failure strains less than 1.0 percent. The analytical and experimental work presented in this study for rock materials uses and extends recently published work on ceramic materials. We particularly cite the experimental and analytical work by Nemat-Nasser *et al.*[5] for pulse shaping and the sample equilibrium model published by Ravichandran and Subhash.[10]

For an ideal Kolsky compression bar experiment, the sample should be in dynamic stress equilibrium and should deform at a constant strain rate over most the duration of the test. To closely approximate these ideal conditions for experiments with brittle ceramic and rock materials, a properly designed, thin copper disk is placed on the impact surface of the incident bar so that a nondispersive ramp pulse propagates in the incident bar. Data from experiments presented in this study show that limestone samples were in equilibrium and at constant strain rates over most of the duration of the tests. Thus, a pulse-shaping technique is an essential modification for closely approximating these ideal test conditions. Experiments that attempt to obtain stress-strain data for ceramic materials at constant strain rates were reported by Rogers and Nemat-Nasser[11] and Chen and Ravichandran.[12] Although we were able to use many of the contributions from the published papers on ceramic materials, several new modifications were required for our Kolsky pressure bar experiments with rock materials. For example, most compressive strengths for ceramics are more than a factor of 10 larger than compressive strengths for limestone, so the limestone sample diameters were the same as the bar diameters. More important, to obtain sample equilibrium, a pulse shaper must be designed to produce a much smaller slope on the ramp pulse propagating in the incident bar because the wave speed for limestone is three to four times as small as typical wave speeds for ceramics. Other critical experimental modifications are discussed in the following sections.

SHPB or Kolsky Bar

As shown in Fig. 1, a conventional SHPB consists of a striker bar, an incident bar, a transmission bar and a sample placed between the incident and transmission bars. A gas gun launches the striker bar at the incident bar, and that impact causes an elastic compression wave to travel in the incident bar toward the sample. When the impedance of the sample is less than that of the bars, an elastic tensile wave is reflected into the incident bar and an elastic compression

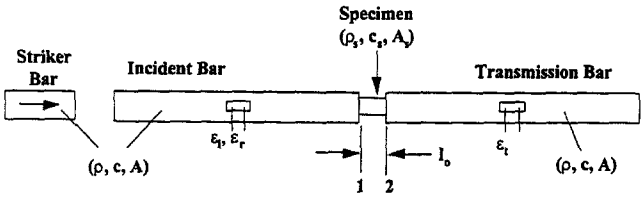

Fig. 1—Schematic of a conventional split Hopkinson pressure bar or Kolsky bar

wave is transmitted into the transmission bar. If the elastic stress pulses in the bars are nondispersive, the elementary theory for wave propagation in bars can be used to calculate the sample response from measurements taken with strain gages mounted on the incident and transmission bars. Strain gages mounted on the incident bar measure the incident ε_i and reflected ε_r strain pulses, and strain gages mounted on the transmission bar measure the transmitted ε_t strain pulse. Nicholas,[3] Follansbee[4] and Gray[7] presented equations that describe the sample response in terms of the measured strain signals.

For this study, the incident and transmission bars were made from the same material with equal cross-sectional areas. As shown in Fig. 1, the bars have density ρ, Young's modulus E, bar wave speed c and cross-sectional area A. Because we focus only on limestone samples that have failure strains less than 1.0 percent, we need only use engineering stress, strain and strain rate measures. In addition, we take stress positive in compression, strain positive in contraction and particle velocity positive to the right in Fig. 1. Figure 1 also shows that the sample has cross-sectional area A_s and length l_o. We take subscripts 1 and 2 to represent the locations of the ends of the sample.

For a homogeneous deformation, the strain rate of the sample is given by

$$\frac{d\varepsilon_s}{dt} = \frac{v_1 - v_2}{l_o}, \tag{1}$$

where v_1 and v_2 are the particle velocities at the sample-bar interfaces. In terms of the measured strain pulses,

$$\frac{d\varepsilon_s}{dt} = \frac{c}{l_o}(\varepsilon_i - \varepsilon_r - \varepsilon_t). \tag{2}$$

Forces at the ends of the sample are

$$P_1 = EA(\varepsilon_i + \varepsilon_r) \tag{3a}$$

$$P_2 = EA\varepsilon_t, \tag{3b}$$

and the average force is

$$P_a = \frac{EA}{2}(\varepsilon_i + \varepsilon_r + \varepsilon_t). \tag{3c}$$

Similarly, stresses at the ends of the sample are

$$\sigma_1 = \frac{EA}{A_s}(\varepsilon_i + \varepsilon_r) \tag{4a}$$

$$\sigma_2 = \frac{EA}{A_s}\varepsilon_t, \tag{4b}$$

and the average sample stress is

$$\sigma_a = \frac{EA}{2A_s}(\varepsilon_i + \varepsilon_r + \varepsilon_t). \tag{4c}$$

If $P_1 = P_2$, the forces on both ends of the sample are equal, and from eqs (3a) and (3b), $\varepsilon_i + \varepsilon_r = \varepsilon_t$. So, if the sample is in dynamic stress equilibrium, the stress, strain rate and strain are given by

$$\sigma_s = \frac{EA}{A_s}\varepsilon_t \tag{5}$$

$$\frac{d\varepsilon_s}{dt} = \frac{-2c}{l_o}\varepsilon_r \tag{6}$$

$$\varepsilon_s = \frac{-2c}{l_o}\int_0^t \varepsilon_r(\tau)d\tau. \tag{7}$$

As discussed in detail by Ravichandran and Subash,[10] Gray[7] and Gray and Blumenthal,[8] eqs (5), (6) and (7) assume that the sample is in dynamic stress equilibrium. Equilibrium should first be examined by comparing the stresses σ_1 and σ_2 at the ends of the sample given by eqs (4a) and (4b). If σ_1 and σ_2 are in reasonable agreement, only then is it reasonable to use eqs (5), (6) and (7) to calculate sample stress, strain rate and strain.

Conventional SHPB or Kolsky Bar Experiment

We present results from a conventional SHPB experiment with an Indiana limestone sample (Elliot Stone Company, Bedford, IN). Pettijohn[13] and Podnieks *et al.*[14] described this limestone as a carbonate rock that contains more than 90 percent calcite and less than 10 percent quartz, has a porosity of about 15 percent and has a grain size ranging between 0.15 mm and 1.0 mm. For this study, the limestone samples had density $\rho_s = 2300$ kg/m^3, Young's modulus $E_s = 24$ GPa and bar wave velocity $c_s = 3200$ m/s. Young's modulus was estimated from quasi-static compression data shown later. In addition, the sample had a length and diameter of 12.7 mm. To maximize the magnitude of the transmitted strain pulse, the sample diameter was made equal to the bar diameter.

The 12.7 mm diameter striker, incident and transmission bars shown in Fig. 1 had lengths of 152 mm, 2130 mm and 915 mm, respectively. The bars were made from high-strength maraging VM350 steel (Vasco Pacific, Montebello, CA) and have density $\rho = 8100$ kg/m^3, Young's modulus $E = 200$ GPa and bar wave velocity $c = 4970$ m/s. The strain gages shown in Fig. 1 are located at 1060 mm from the impact surface on the incident bar and 229 mm from the sample-bar interface on the transmission bar.

Figure 2 shows incident, reflected and transmitted strain-time signals for a striking velocity of 8.05 m/s. The incident pulse has a fast rise time of about 10 μs and a pulse width of about 60 μs that correspond to two wave transit times in the striker bar. Figure 3 shows stress versus time at the ends of the sample calculated from eqs (4a) and (4b) and the average strain rate calculated from eq (2). For an ideal SHPB experiment, the sample should be in equilibrium and should deform at a constant strain rate over most of the duration of the test. However, Fig. 3 shows that σ_1 and σ_2 are not in

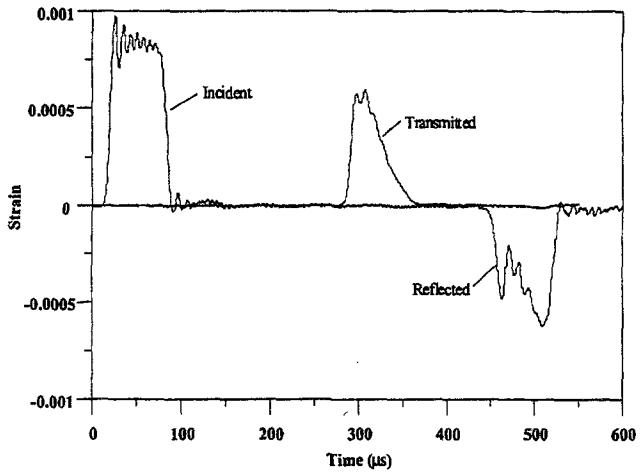

Fig. 2—Strain-time signals for a conventional split Hopkinson pressure bar experiment with a limestone sample

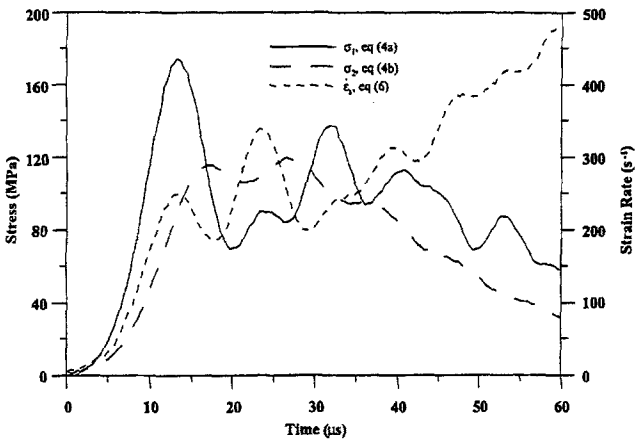

Fig. 3—Interface stresses and strain rate from a conventional split Hopkinson pressure bar experiment with a limestone sample

close agreement and that the strain rate is not constant over the duration of the test.

In the next sections, we present models and experimental results that show a ramp incident pulse is required to obtain sample equilibrium and constant strain rate over most of the test duration. The ramp incident pulse is produced by placing a thin copper disk on the impact surface of the incident bar. We describe the details of this pulse-shaping technique in another study.[15]

Models for Sample Equilibrium and Constant Strain Rate

In this section, we develop models that show the evolutionary process for sample equilibrium and constant strain rate for brittle materials that have a linear stress-strain response until failure. These models and subsequent experiments show that a ramp stress pulse in the incident bar is required to obtain sample equilibrium and constant strain rate over most of the duration of the experiment. The first model assumes that the sample is in dynamic stress equilibrium and predicts strain and strain rate versus time. For the second model, we perform a wave propagation analysis on the interaction of the sample with the incident and transmission bars. This second model predicts the stress-time histories on either side of the sample.

A ramp pulse propagates in the incident bar given by

$$\sigma_i(x,t) = M \cdot (t - x/c) \cdot H(t - x/c), \tag{8}$$

where H is the Heaviside unit function and M is the stress-loading rate. We take $x = 0$ at the interface between the incident bar and the sample labeled as station 1 in Fig. 1. If the sample is in equilibrium, $\sigma_1 = \sigma_2$, we can neglect wave propagation in the sample. The sample is assumed to have a linear stress-strain response to failure given by

$$\sigma_s = E_s \varepsilon_s, \tag{9}$$

where E_s is the Young's modulus for the sample.

When the incident stress pulse reaches the sample, a tensile pulse is reflected back into the incident bar and a compressive pulse is transmitted into the transmission bar. As before, we take stress positive in compression, strain positive in contraction and particle velocity positive to the right in Fig. 1. From the equations of elementary bar theory,[16] strain rate in the sample given by eq (1) can be written in terms of the incident σ_i, reflected σ_r and transmitted σ_t stress pulses in the bars as

$$\frac{d\varepsilon_s}{dt} = \frac{1}{\rho c l_o}(\sigma_i - \sigma_r - \sigma_t). \tag{10}$$

For a sample in equilibrium, $\sigma_i + \sigma_r = \sigma_t$, and

$$\frac{d\varepsilon_s}{dt} = \frac{2}{\rho c l_o}(\sigma_i - \sigma_t). \tag{11}$$

The incident and transmitted stresses in the bars are

$$\sigma_i = Mt \tag{12a}$$

$$\sigma_t = \frac{A_s E_s \varepsilon_s}{A}. \tag{12b}$$

From eqs (11) and (12),

$$\frac{d\varepsilon_s}{dt} + \frac{2A_s E_s}{\rho c A l_o}\varepsilon_s = \frac{2Mt}{\rho c l_o}, \tag{13}$$

which has solutions

$$\frac{d\varepsilon_s}{dt} = \frac{\gamma M}{E_s}\left[1 - \exp\left(\frac{-2t}{r t_o}\right)\right] \tag{14a}$$

$$\varepsilon_s = \frac{\gamma M}{E_s}\left\{t - \frac{r t_o}{2}\left[1 - \exp\left(\frac{-2t}{r t_o}\right)\right]\right\} \tag{14b}$$

$$\gamma = \frac{A}{A_s} \quad r = \frac{A\rho c}{A_s \rho_s c_s} \quad t_o = \frac{l_o}{c_s}. \tag{14c}$$

Equations (14a) and (14b) give closed-form solutions for the strain rate and strain in the sample. However, this model assumes that the sample is in equilibrium.

For the second model, we perform a wave propagation analysis on the interaction of the sample with the incident and transmission bars. Ravichandran and Subhash[10] presented a method-of-characteristics solution for this problem and show results for ceramic materials. Our analysis of this

same problem provides general, closed-form equations that we find more convenient for numerical applications.

We use the elementary theory of wave propagation in bars to calculate the stress-time histories at the ends of the sample. Ravichandran and Subhash[10] and Graff[16] presented equations for the reflected and transmitted stresses at the interfaces shown in Fig. 1. At the incident bar-sample interface (location 1 in Fig. 1), the stresses transmitted to the specimen σ_t and reflected in the incident bar σ_r are

$$\sigma_t = \left(\frac{2\gamma}{r+1}\right)\sigma_i \tag{15a}$$

$$\sigma_r = -\left(\frac{r-1}{r+1}\right)\sigma_i, \tag{15b}$$

in which r is given by eq (14c) and σ_i is the incident pulse given by eq (8). We take $x = 0$ at station 1 in Fig. 1, and the stress in the sample at station 1 is

$$\sigma_1 = \frac{2\gamma M t}{r+1} \quad 0 \le t < 2t_o. \tag{16}$$

At $t = t_o$, the stress wave in the sample reaches the sample-transmission bar interface (location 2 in Fig. 1). When the stress wave in the sample interacts with the transmission bar, the stresses transmitted into the transmission bar σ_t and reflected into the sample are

$$\sigma_t = \frac{2r}{\gamma(r+1)}\ \sigma_1(t-t_0),\ t_o \le t < 3t_o \tag{17a}$$

$$\sigma_r = \left(\frac{r-1}{r+1}\right)\ \sigma_1(t-t_0),\ t_o \le t < 3t_o, \tag{17b}$$

where σ_1 is given by eq (16). The stress in the sample at station 2 consists of the incident and reflected stress waves and is given by

$$\sigma_2(t) = \frac{2\gamma M}{r+1}(t-t_o) + \left(\frac{r-1}{r+1}\right)\frac{2\gamma M}{r+1}(t-t_o) \quad t_o \le t < 3t_o. \tag{18}$$

We repeat this interaction process several times and obtain

$$\sigma_1 = \frac{2\gamma M t}{r+1} \quad 0 \le t < 2t_o \tag{19a}$$

$$\sigma_1 = \frac{2\gamma M}{r+1}\left\{t + \left[\left(\frac{r-1}{r+1}\right) + \left(\frac{r-1}{r+1}\right)^2\right](t-2t_o)\right\} \quad 2t_o \le t < 4t_o \tag{19b}$$

$$\sigma_1 = \frac{2\gamma M}{r+1}\left\{t + \left[\left(\frac{r-1}{r+1}\right) + \left(\frac{r-1}{r+1}\right)^2\right](t-2t_o) + \left[\left(\frac{r-1}{r+1}\right)^3 + \left(\frac{r-1}{r+1}\right)^4\right](t-4t_o)\right\} \quad 4t_o \le t < 6t_o \tag{19c}$$

and

$$\sigma_2 = 0 \qquad 0 \le t < t_o \tag{20a}$$

$$\sigma_2 = \frac{2\gamma M}{r+1}\left\{\left[1 + \left(\frac{r-1}{r+1}\right)\right](t-t_o)\right\} \quad t_o \le t < 3t_o \tag{20b}$$

$$\sigma_2 = \frac{2\gamma M}{r+1}\left\{\left[1 + \left(\frac{r-1}{r+1}\right)\right](t-t_o) + \left[\left(\frac{r-1}{r+1}\right)^2 + \left(\frac{r-1}{r+1}\right)^3\right](t-3t_o)\right\} \quad 3t_o \le t < 5t_o. \tag{20c}$$

The nth term for eqs (19) and (20) is

$$\frac{2\gamma M}{r+1}\left[\left(\frac{r-1}{r+1}\right)^{n-1} + \left(\frac{r-1}{r+1}\right)^n\right](t-nt_o)$$

for the time interval $nt_o \le t < (n+2)t_o$. Therefore, σ_1 and σ_2 can easily be calculated for times greater than those given by eqs (19) and (20).

Figure 4 shows model predictions for sample stresses and strain rate versus time. These predictions correspond to experiments with steel bars and limestone samples ($r = 5.5$) and with equal sample and bar diameters ($\gamma = 1$). For Fig. 4, the stress-loading rate in the incident bar is $M = 3.3$ MPa/μs and corresponds to the loading rate for experiments discussed in the next section. In addition, the sample fails or starts to fail at a sample stress of about 120 MPa. Figure 4 shows that the stresses at the incident bar-sample interface σ_1 and the sample-transmission bar interface σ_2 are nearly equal for $t/t_o > 2$. In addition, the sample stress predicted by the model that assumes sample equilibrium given by eqs (9) and (14b) lies between σ_1 and σ_2. The strain rate rapidly increases from $0 < t/t_o < 4$ and is nearly constant for $4 < t/t_o < 12$, so the strain rate is nearly constant for a sample stress between about 20 MPa and 120 MPa.

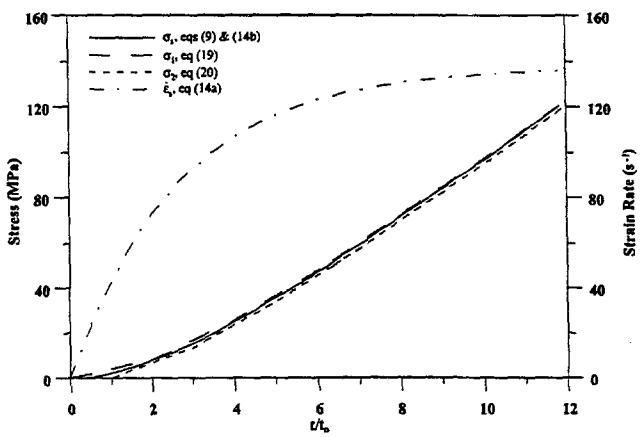

Fig. 4—Stress and strain rate model predictions for a limestone sample loaded by a ramp incident pulse with a stress loading rate of 3.3 MPa/μs

Modified SHPB or Kolsky Compression Bar Experiments

Models developed in the previous section predict that a nondispersive ramp pulse in the incident bar is required for testing brittle materials that have a linear stress-strain response to failure. To obtain the ramp pulse in the incident bar, we modify the conventional SHPB technique by placing a thin copper disk on the impact surface of the incident bar. Nemat-Nasser *et al.*[5] presented a pulse-shaping model and data for oxygen-free, high-purity copper (C10200).[17] In another study,[15] we extended the model of Nemat-Nasser *et al.* and presented data for both annealed and hardened (C11000)[17] copper pulse shapers.

In this section, we present results from two experiments that demonstrate our modified SHPB technique. Data from experiments with limestone show that the samples are in dynamic stress equilibrium and have nearly constant strain rates over most of the duration of the tests. In addition, we carefully bracket sample failure with one test where the sample fails with catastrophic damage and a second test where the sample is recovered intact. These experiments used the same limestone samples described earlier. The sample had a length and diameter of 12.7 mm, and the sample and bar diameters were equal. The high-strength steel incident and transmission bars had lengths of 2130 mm and 915 mm, respectively. Strain gages shown in Fig. 1 are located at 1065 mm from the impact surface of the incident bar and 229 mm from the sample-bar interface on the transmission bar. To obtain a nearly linear ramp pulse in the incident bar, a 3.97 mm diameter, 0.79 mm thick annealed (C11000)[15,17] copper disk was placed on the impact surface of the incident bar. All the above-mentioned parameters remained fixed for the two experiments presented in this section. However, the first experiment used a 152 mm long steel striker bar, and the second experiment used a 51 mm long steel striker bar. Both striker bars were launched to a striking velocity of 13.9 m/s.

Figure 5 shows the measured incident stress pulse and a prediction from our model[15] for a 152 mm long steel striker bar with a striking velocity of 13.9 m/s. Note that the incident stress pulse is nearly a linear ramp for about 75 μs and has a stress-loading rate of about $M = 3.3$ MPa/μs. Incident, reflected and transmitted strain pulses presented in Fig. 6 show that the high-frequency oscillations that appear in Fig. 2 are eliminated with pulse shaping. Thus, data analyses that use the elementary bar theory should be more accurate for pulse-shaped experiments. Figure 7 presents stresses in the sample at the incident bar-sample interface σ_1 and the sample-transmission bar interface σ_2 calculated from eqs (4a) and (4b) that use the measured strain signals. We also show that the model prediction from eqs (9) and (14b) are in good agreement with the measured stresses and that σ_1 and σ_2 are in close agreement. Thus, the sample is nearly in a state of dynamic stress equilibrium. Figure 7 also shows the predicted and measured strain rates versus time. Strain rate is nearly constant for 15 μs $< t <$ 50 μs. At about 50 μs, the limestone sample begins to fail. When failure starts, the sample is no longer in a state of homogeneous deformation, and the valid range of the experiment is over. Posttest observations showed that the sample eventually experienced catastrophic damage.

Figures 5 and 7 show that the incident ramp pulse was loading for about 75 μs and that the limestone sample started

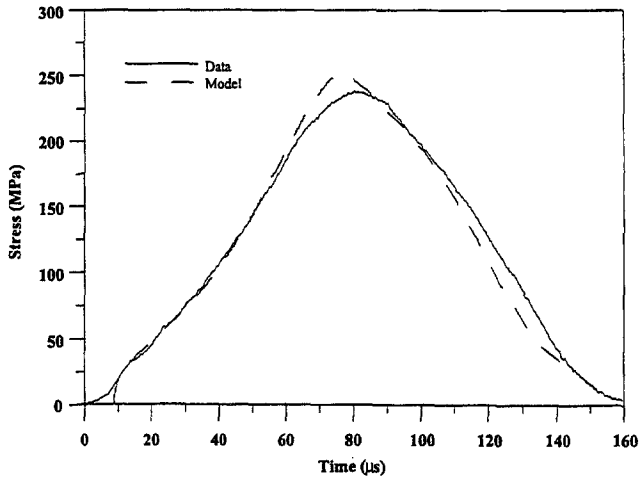

Fig. 5—Data and model prediction for an incident pulse with an annealed copper pulse shaper

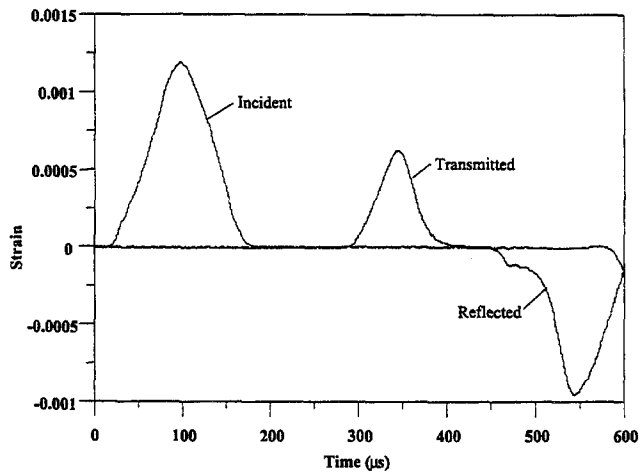

Fig. 6—Strain-time signals for a pulse-shaped split Hopkinson pressure bar experiment with a limestone sample

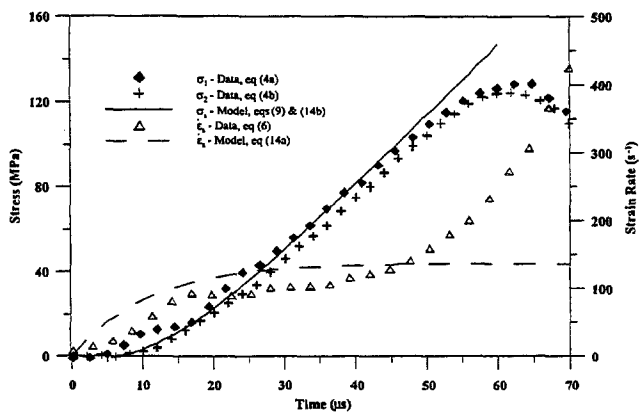

Fig. 7—Interface stresses and strain rate from a pulse-shaped split Hopkinson pressure bar experiment with a limestone sample

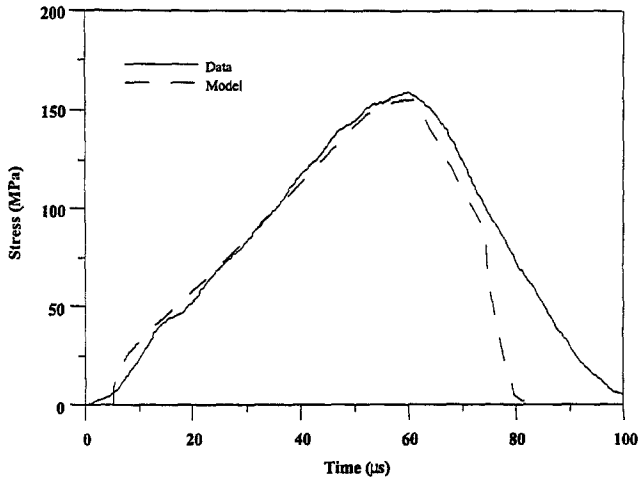

Fig. 8—Data and model prediction for an incident pulse with an annealed copper pulse shaper

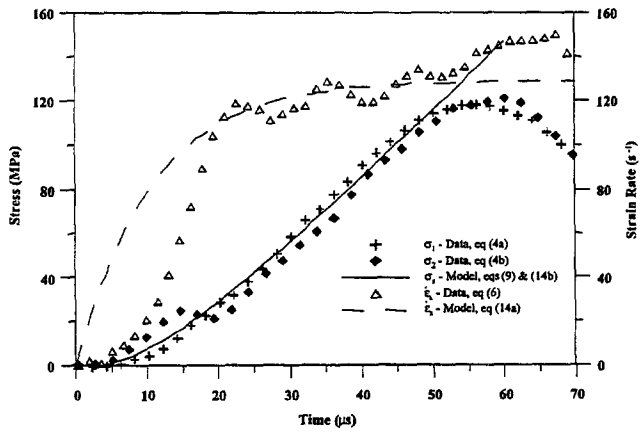

Fig. 9—Interface stresses and strain rate from a pulse-shaped split Hopkinson pressure bar experiment with a limestone sample

to fail at about 50 μs. Therefore, the sample continued to be loaded after the start of failure and eventually experienced catastrophic damage. To recover an intact limestone sample after a test, we conducted another experiment in which the duration of the ramp pulse in the incident bar was shorter than that shown in Fig. 5. Figure 8 shows the measured incident stress pulse and a prediction from our model[15] for a 51 mm long steel striker bar with a striking velocity of 13.9 m/s. Note that the incident stress pulse is nearly a linear ramp for about 50 μs and has a stress-loading rate of about $M = 3.1$ MPa/μs. Thus, the incident pulses shown in Figs. 5 and 8 are almost identical except for the loading durations of 75 μs and 50 μs, respectively. Results for the 50 μs ramp incident pulse are shown in Fig. 9 and are very similar to those presented in Fig. 7. However, the strain rate in Fig. 7 shows an exponential growth after about 50 μs, and the strain rate in Fig. 9 remains nearly constant. Thus, the sample is loaded after failure began in the first experiment, and the loading ended at about the time the sample started to fail in the second experiment. In the first experiment, the limestone sample eventually failed with catastrophic damage, whereas in the second experiment, the sample was recovered intact. From Figs. 7 and 9, we conclude that the limestone sample has a failure stress of about 120 MPa for a strain rate between 100 s^{-1} and 120 s^{-1}.

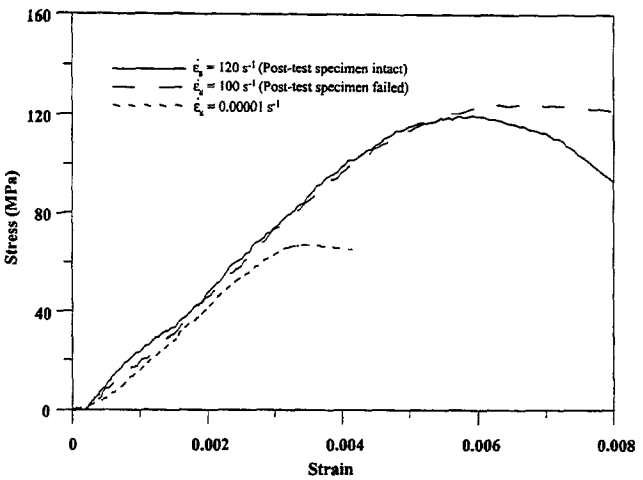

Fig. 10—Quasi-static and dynamic stress-strain data

In Fig. 10, we show stress-strain curves from the dynamic experiments discussed in this section and a quasi-static stress-strain curve. We note that the failure stress at a strain rate between 100 s^{-1} and 120 s^{-1} is about double that obtained from a quasi-static experiment.

Effect of Strain Rate on the Compressive Strength of Indiana Limestone

We conducted unconfined compression experiments with the Indiana limestone samples for strain rates between 10^{-5} and 300 s^{-1}. Thirty-one experiments were conducted in servohydraulic load frames for strain rates to about 4 s^{-1}, and nine experiments were conducted with our new SHPB technique for strain rates greater than 10 s^{-1}. Because the compressive strength of some rock materials has been shown[18] to be dependent the length-to-diameter (L/D) ratio and size of the samples tested, we present data for several specimen geometries in Fig. 11. The servohydraulic data include eight experiments conducted by Olsson and Mosher[19] on 25.4 mm diameter by 50.8 mm long samples. We conducted the other experiments on 12.7 mm diameter samples with L/D varying from 1 to 2. Unlike much of the rock data discussed by Farmer,[18] the compressive strength of this Indiana limestone does not show an L/D or size effect. In addition, the data in Fig. 11 show that the compressive strength of Indiana limestone increases with increasing strain rate.

Conclusions

We presented a modified SHPB or Kolsky bar technique to obtain compressive stress-strain data for rock materials. A nondispersive ramp pulse was produced in the incident bar by placing a thin copper disk on the impact surface of the incident bar. Data from experiments with limestone samples showed that the samples were in dynamic stress equilibrium and had constant strain rates over most of the test durations. In addition, we showed that the ramp pulse durations could be controlled such that samples unloaded just prior to failure. Thus, intact samples that experienced strains beyond the elastic region and postpeak stresses could be retrieved for microstructural evaluations. Compressive failure stress data for strain rates between 10^{-5} and 300 s^{-1} showed an increase in compressive strength as strain rate increased. We also

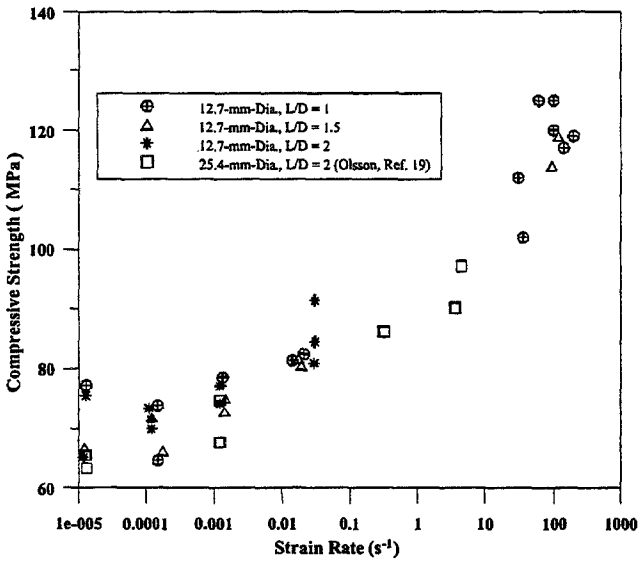

Fig. 11—Strain rate sensitivity of the compressive strength of Indiana limestone

presented analytical models that predicted the time durations for sample equilibrium and constant strain rate.

Acknowledgments

This work was sponsored by the U.S. Army Engineer Research and Development Center (ERDC) at the Waterways Experiment Station under a laboratory director's discretionary research program and by the Sandia National Laboratories Joint DoD/DOE Penetration Technology Program. Sandia is a multiprogram laboratory operated by Sandia Corporation, a Lockheed Martin Company, for the U.S. Department of Energy under Contract No. DE-AC04-94AL8500. The authors gratefully acknowledge permission from the director of the Structures Laboratory at ERDC to publish this work.

References

1. Kolsky, H., "An Investigation of the Mechanical Properties of Materials at Very High Rates of Loading," Proc. Roy. Soc. Lon. B, **62**, *676–700 (1949).*

2. Kolsky, H., Stress Waves in Solids, Dover, New York (1963).

3. Nicholas, T., "Material Behavior at High Strain Rates," Impact Dynamics, John Wiley & Sons, New York, Chap. 6 (1982).

4. Follansbee, P.S., "The Hopkinson Bar," Mechanical Testing, Metals Handbook, 9th ed., **8**, *American Society for Metals, Metals Park, OH, 198–217 (1985).*

5. Nemat-Nasser, S., Isaacs, J.B., and Starrett, J.E., "Hopkinson Techniques for Dynamic Recovery Experiments," Proc. Roy. Soc. Lon. A, **435**, *371–391 (1991).*

6. Ramesh, K.T. and Narasimhan, S., "Finite Deformations and the Dynamic Measurement of Radial Strains in Compression Kolsky Bar Experiments," Int. J. Solids Struct., **33**, *3723–3738 (1996).*

7. Gray, G.T., "Classic Split-Hopkinson Pressure Bar Technique," LA-UR-99-2347, Los Alamos National Laboratory (1999).

8. Gray, G.T. and Blumenthal, W.R., "Split-Hopkinson Pressure Bar Testing of Soft Materials," LA-UR-99-4878, Los Alamos National Laboratory (1999).

9. Yadav, S., Chichili, D.R., and Ramesh, K.T., "The Mechanical Response of a 6061-T6 Al/Al2O3 Metal Matrix Composite at High Rates of Deformation," Acta Metall. Mat., **43**, *4453–4464 (1995).*

10. Ravichandran, G. and Subhash, G., "Critical Appraisal of Limiting Strain Rates for Compression Testing of Ceramics in a Split Hopkinson Pressure Bar," J. Am. Cer. Soc., **77**, *263–267 (1994).*

11. Rogers, W.P. and Nemat-Nasser, S., "Transformation Plasticity at High Strain Rate in Magnesia-partially-stabilized Zirconia," J. Am. Cer. Soc., **73**, *136–139 (1990).*

12. Chen, W. and Ravichandran, G., "Dynamic Compressive Failure of a Glass Ceramic under Lateral Confinement," J. Mech. Phys. Solids, **45**, *1303–1328 (1997).*

13. Pettijohn, E.R., Sedimentary Rocks, 3d ed., Harper & Row, New York (1975).

14. Podnieks, E.R., Chamberlain, P.G., and Thill, R.E., "Environmental Effects on Rock Properties," Proceedings of Tenth Symposium on Rock Mechanics, American Institute of Mechanical Engineers, New York, 215–241 (1972).

15. Frew, D.J., Forrestal, M.J., and Chen, W., "Pulse Shaping Techniques for Testing Brittle Materials with a Split Hopkinson Pressure Bar," Unpublished manuscript.

16. Graff, K.F., Wave Motions in Elastic Solids, Dover, New York (1975).

17. Lewis, C. F., "Properties and Selection : Nonferrrous Alloys and Pure Metals," In Metals Handbook, 9th Edition, 2, American Society for Metals, Metals Park, OH (1979).

18. Farmer, I., Engineering Behavior of Rocks, 2nd Edition, Chapman and Hall, New York (1983).

19. Olsson, B. and Mosher, D., Sandia National Laboraories, Albuquerque, NM. Unpublished notes sent to M. J. Forrestal, November (1996).